Shu, Q., Chang, Z., and Mavrogenes, J., Fluid compositions reveal fluid nature, metal deposition mechanisms, and mineralization potential: An example at the Haobugao Zn-Pb skarn, China.

Supplementary Online Materials

(This PDF file includes Analytical methods and results for fluid inclusions and Figures S1–S6. Note that the data sources including Tables S1–S6 are in another Data Repository Excel file.)

1. Supplementary text

1.1. Analytical methods for fluid inclusions

Fluid inclusion microthermometry

Qualitative determination for single fluid inclusion composition was conducted using a RM-1000 Laser Raman probe at Peking University, China, with a laser wavelength of 514.5 nm, a laser power of 20 mW, a diameter of laser beam spot of 2 μm, and a spectrometer resolution of 2 cm^{-1}. Microthermometric data were collected using an INSTEC HCS622XY programmable heating-cooling stage attached to a Nikon ECLIPSE LV100POL transmitted light microscope. The stage was calibrated using synthetic fluid inclusions at -56.6, 0 and 374 ℃. Estimated accuracy was ±0.1 ℃ for measurements of final ice-melting temperatures and ±4 ℃ for halite dissolution and final homogenization temperatures (Th). A Microsoft excel spreadsheet from Steele-MacInnis et al. (2012), $H_{OKIE}F_{LINCS}$_H2O-N_AC_L, was used to calculate the salinities of the fluid inclusions.

Fluid inclusion LA-ICP-MS composition analysis

In-situ analysis of single fluid inclusion compositions using LA-ICP-MS was conducted at the Advanced Analytical Centre, James Cook University, Australia. The detailed procedure has been described in Hammerli et al. (2013) and Shu et al. (2017). Individual inclusions were ablated with a Geolas Pro 193 nm ArF excimer laser system in helium gas. The helium carrier gas was mixed with argon gas before sample aerosol was introduced into the Varian 820 quadrupole ICP-MS. The laser beam diameter was adjusted for each analysis to ensure complete ablation of the fluid inclusion while minimizing the blasting of the host mineral. The analyses were carried out with laser spots of 16, 24, 32 or 44 μm, depending on the fluid inclusion sizes. The laser was turned on after measuring a gas blank for ~35 seconds for each spot. The first section of the signals was from the host mineral. Once a fluid inclusion was reached and opened, the mixed signals of the fluid inclusion and the host mineral were collected.

The composition of the host mineral was reduced from the same spot analysis for a fluid inclusion based on the mineral signals in each analysis. The external standard was NIST610, and the internal standards were Ca for pyroxene, Zn for sphalerite, and stoichiometric Ca (40 wt%) for calcite. Electron microprobe analyses revealed that the Zn content in sphalerite ranges from 56.44 to 61.95 wt% (59.50 ±1.75 wt%, n = 24), with only minor variations. Pyroxene is composed of 48.05–54.76 wt % SiO_2, 22.22–26.41 wt % CaO, 0.37–18.35 wt % MgO, 0.61–22.27 wt % FeO, and 0.13–8.00 wt % MgO (n = 26). The CaO contents are relatively homogenous with an average

of 23.79 ± 1.54, and therefore Ca can be reliably used as the internal standard.

It was not practical to carry out microthermometric measurement of every fluid inclusion prior to LA-ICP-MS analysis. Therefore the average salinity of the measured fluid inclusions in one fluid inclusion assemblage (FIA) has been used to represent the salinity of all the individual inclusions in the FIA (e.g., Shu et al., 2017). This is justified by the fact that in a given FIA the fluid inclusions have similar salinities with only slight variations (Table S2). The concentration of Na derived from the average NaCl wt% equivalent value of a given fluid inclusions assemblage and corrected for contribution of other chloride salts by the empirical algorithm proposed by Allan et al. (2005), was used as the internal standard to transform the element mass ratios into absolute concentrations. Matrix correction was based on the equation by Halter et al. (2002). The reference elements are Zn for fluid inclusions in sphalerite, and Ca for those in calcite and pyroxene. All the data reduction was performed using the SILLS software package (Guillong et al., 2008).

The concentrations of Si, Ca, Mg, Mn and Fe in pyroxene are typically high; so are Zn, Fe, Mn and Ag in sphalerite, and Ca, Fe, Mn and Sr in calcite. These elements in the fluid inclusions hosted in the corresponding minerals could not be precisely measured due to the high matrix contributions. Other elements selected for analyses have all been well quantified, including Li, Na, K, Cu, Zn, As, Rb, Mo, Sn, Cs, Ba, and Pb in fluid inclusions hosted in all three types of minerals, Zn and Ag in pyroxene- and calcite-hosted inclusions, Sr in pyroxene- and sphalerite-hosted inclusions, and Ca in sphalerite-hosted inclusions.

1.2. Fluid inclusion data

Fluid inclusion microthermometry

Laser Raman spectroscopic analyses were conducted on all the above four fluid inclusion types prior to microthermometric and LA-ICP-MS analyses. The results suggest that both the liquid and vapor phases of these inclusions are almost solely H_2O, with no other detectable gases such as CO_2 or CH_4. Therefore, the salinities of all the inclusions were calculated assuming a simple NaCl-H_2O system (Steele-MacInnis et al., 2012). All salinity data were reported as wt% NaCl equivalent. The microthermometric results are listed in Table S2 and summarized in Fig. S4.

Pyroxene-hosted fluid inclusions. Type B and V inclusions were all from prograde stage pyroxene. For the 19 Type B FIAs, the halite crystals homogenized exclusively prior to the vapor bubble at 263–382 ℃ during heating. The calculated salinities derived from halite dissolution temperatures range from 35.4 to 45.3 wt% NaCl equivalent. Homogenization by vapor disappearance occurred at 421–575 ℃ (Table S2). For Type V inclusions, the final ice melting and/or homogenization were difficult to observe due to their large bubble and unclear phase boundary, and only three FIAs have been successfully measured in this study. Salinities of the three FIAs are 7.1, 3.9 and 4.1 wt% NaCl equivalent, based on the ice-melting temperatures -4.5, -2.4 and -2.5 ℃. These individual Type V inclusions homogenized to vapor phase, and the average Th for the three FIAs are 476, 491, and 448 ℃.

Sphalerite- and calcite-hosted Type L fluid inclusions. All measured fluid inclusions in sphalerite are Type L inclusions. The 11 FIAs yielded average ice-melting temperatures between -1.8 and -6.2 ℃, corresponding to salinities of 3.0–9.5 wt% NaCl equivalent. Average Th are 240–369 ℃ (Table S2). The calcite coexistent with the Zn-Pb sulfides share similar fluid inclusion microthermometric results. The nine analyzed Type L FIAs in calcite have ice-melting temperatures from -1.3 to -3.9 ℃, corresponding to salinities of 2.2–6.2 wt% NaCl equivalent.

The measured Th are 257–360 ℃ (Table S2).

Calcite-hosted Type SL fluid inclusions. Type SL in calcite generally have lower Th and salinities, and are believed to represent the spent fluids after the Zn-Pb mineralization. The ice-melting temperatures of five FIAs range from -0.7 to -2.5 ℃, corresponding to salinities of 1.2–4.2 wt% NaCl equivalent. The Th are 152–204 ℃ (Table S2).

Fluid compositions

Pyroxene-hosted fluid inclusions. The average concentration of Na in each FIA was used as the internal standard, ranging from 5.4 to 12.3 wt% for the Type B FIAs in pyroxene. LA-ICP-MS analysis reveals that the K content ranges from 4.3 to 11.8 wt%, with K/Na mass ratios varying between 0.3 and 2.5. The concentrations of the two major metals are 0.5–1.4 wt% Zn and 0.5–1.8 wt% Pb, respectively. The concentration ranges of other elements are 561–3128 ppm Li, 145–880 ppm As, 174–421 ppm Cu, 21–84 ppm Mo, 38–92 ppm Ag, 27–122 ppm Sn, 268–1011 ppm Sr, 535–1247 ppm Rb, 404–1714 ppm Cs, and 139–618 ppm Ba (Tables S3–S4; Fig. S4).

The average Na concentrations for the three Type V FIAs are 1.8, 1.1, and 0.9 wt%. The average concentrations of K, Zn and Pb are 1.0, 0.08, and 0.11 wt%, respectively. The average concentrations of other elements are 556 ppm Li, 187 ppm As, 114 ppm Cu, 12 ppm Mo, 7 ppm Ag, 6 ppm Sn, 132 ppm Sr, 122 ppm Rb, 137 ppm Cs, and 60 ppm Ba.

Sphalerite- and calcite-hosted Type L fluid inclusions. The 11 FIAs in sphalerite contain 0.3–1.7 wt% Na, 0.2–2.0 wt% K and 0.4–0.9 wt % Ca, with K/Na ratios varying from 0.2 to 1.2, and Ca/K ratios of 0.3–1.9. The average Pb concentrations are 12–1266 ppm with an average of 236 ppm, significantly lower than that in the pyroxene-hosted Type B FIAs (0.5–1.8 wt% with an average of 1.0 wt%). The concentrations of other elements, when detected, show insignificant variations among individual inclusions, and the average concentrations for the 11 FIAs are 35–327 ppm Li, 16–71 ppm As, 31–451 ppm Cu, 3–13 ppm Mo, 2–22 ppm Sn, 24–159 ppm Sr, 34–199 ppm Rb, 36–210 ppm Cs, and 10–60 ppm Ba (Tables S3–S4; Fig. S4).

In calcite, the Type L FIAs have 0.6–1.8 wt% Na (n = 9) and 0.4–1.3 wt% K, with K/Na ratios of 0.4–1.1. The average Zn and Pb concentrations are 57–1220 and 27–1558 ppm, respectively. The average concentrations of other elements are 34–238 ppm Li, 14–55 ppm As, 26–132 ppm Cu, 1–10 ppm Mo, 2–18 ppm Ag, 3–15 ppm Sn, 28–144 ppm Rb, 29–224 ppm Cs, and 8–52 ppm Ba.

Generally, fluid inclusions hosted in syn-ore stage sphalerite and calcite are very similar in salinity, temperature and composition (Tables S3–S4; Figs. S4–S5). For example, the analyzed samples H12-8 and H12-1 contains coexistent sphalerite and calcite, and the trapping temperatures, fluid salinities, and element concentrations in both minerals are highly comparable, and are mostly plotted on or near the 1:1 lines (Fig. S5). This further confirms that the Zn-Pb mineralization stage calcite and sphalerite were precipitated from the same fluids.

Calcite-hosted Type SL fluid inclusions. Secondary Type SL FIAs in calcite have average Na contents of 0.4–1.0 wt% (n = 5) and K of 0.2–0.8 wt%, with K/Na ratios of 0.5–0.9. The average concentrations of Li, Rb, Cs, Ba and Pb are 90–178, 11–56, 15–121, 10–26, and 15–22 ppm, respectively. Copper, Zn, As and Ag were only detected in one FIA, and are 31, 31, 11 and 4 ppm, respectively. Other elements including Sn and Mo are below the detection limits (Tables S3–S4; Fig. S4).

2. Supplementary Figures

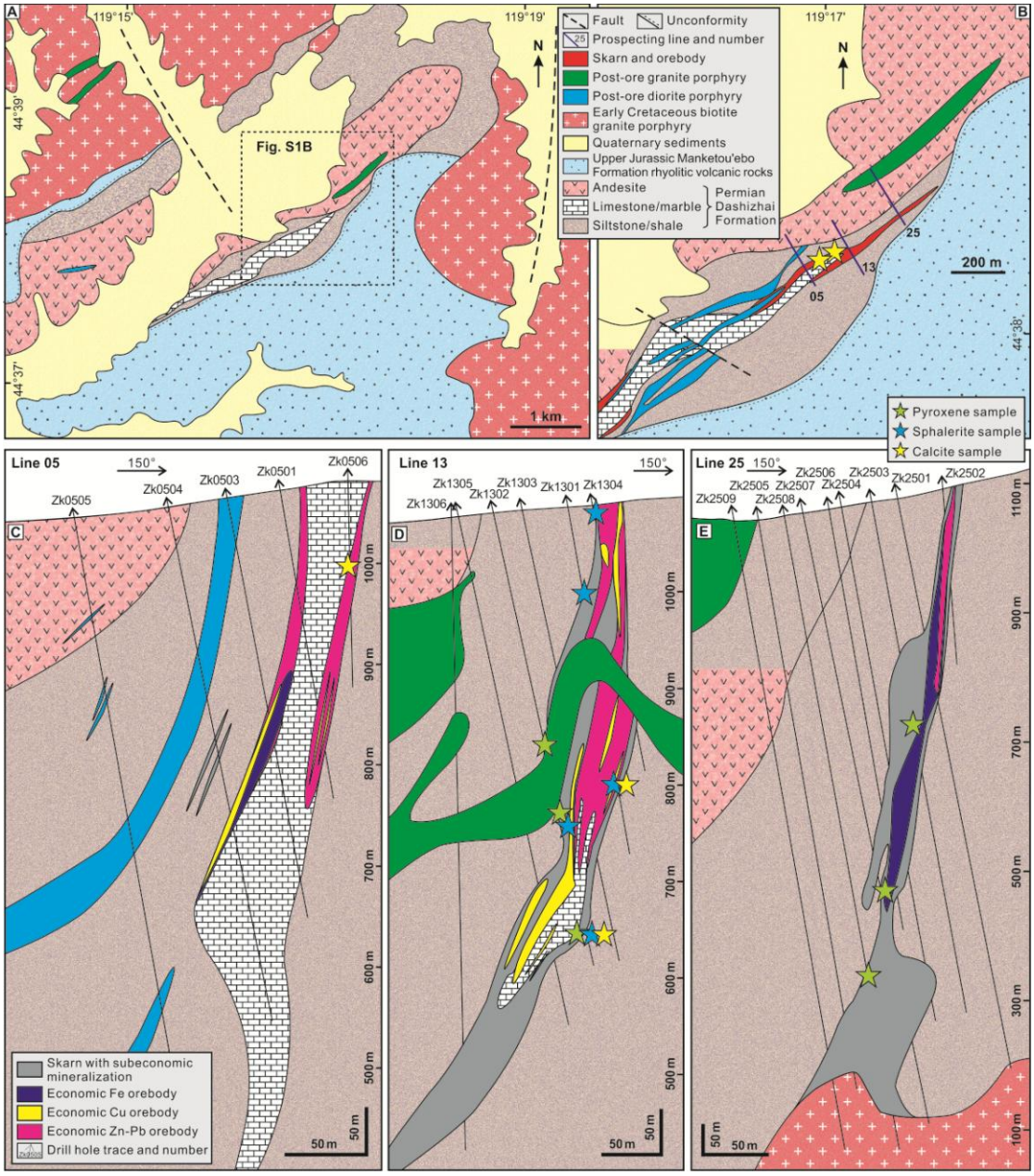

Figure S1 Simplified geological map of Haobugao and its adjacent areas (A). Geological map of the Haobugao Zn-Pb deposit (B; after Li, 2015). Representative geological cross sections through the Haobugao Zn-Pb deposit showing the spatial relationship among different stratigraphy units, intrusions, and skarn and orebodies (C, D and E; modified after Li, 2015 and Liu et al., 2018). Locations of samples used for fluid inclusion analyses including these from surface and drill cores are shown by stars. Details of these samples are given in Table S1.

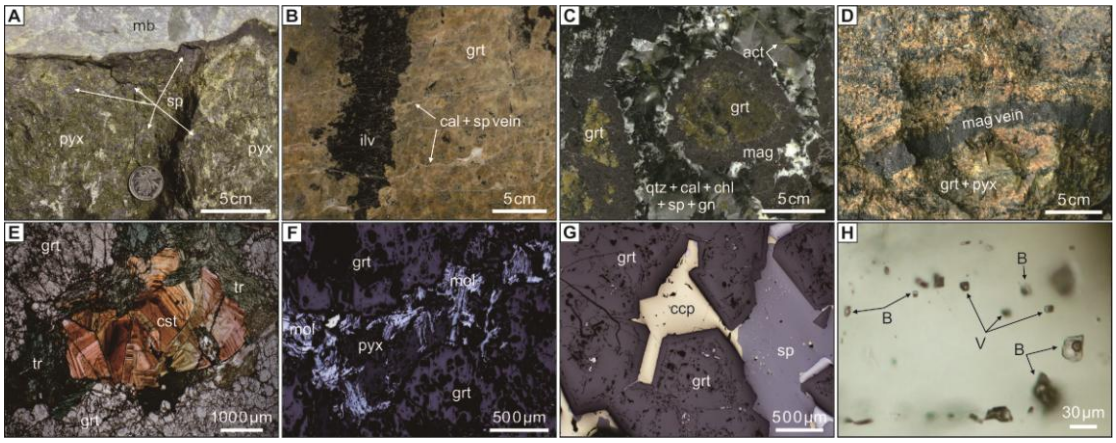

Figure S2 Supplemental photographs (A–D) and photomicrographs (E–H) showing representative mineral assemblages and fluid inclusions in the Haobugao Zn-Pb deposit. A: Distal pyroxene skarn near marble; note pyroxene is postdated by sphalerite (sp). B: Ilvaite (ilv) cutting massive garnet skarn, and is cut by later sphalerite-calcite (cal) veins. C: Magnetite (mag) replacing garnet, with later interstitial quartz (qtz)-calcite-chlorite (chl)-actinolite (act)-sphalerite-galena (gn). D: Magnetite vein cutting massive garnet-pyroxene skarn. E: Retrograde tremolite (tr) and cassiterite (cst) postdating prograde garnet skarn (photo provided by L.J. Liu through personal communication). F: Massive garnet-pyroxene skarn cut by molybdenite (mol) veins. G: Sphalerite-chalcopyrite filling the interstices between garnet crystals. E: Assemblage with coexisting Type B and Type V fluid inclusions in pyroxene. Note that based on these mineral assemblages shown here and those in Figure 1 in the main text, the hydrothermal event in Haobugao can temporally be divided into four stages as shown in Figure S3 below.

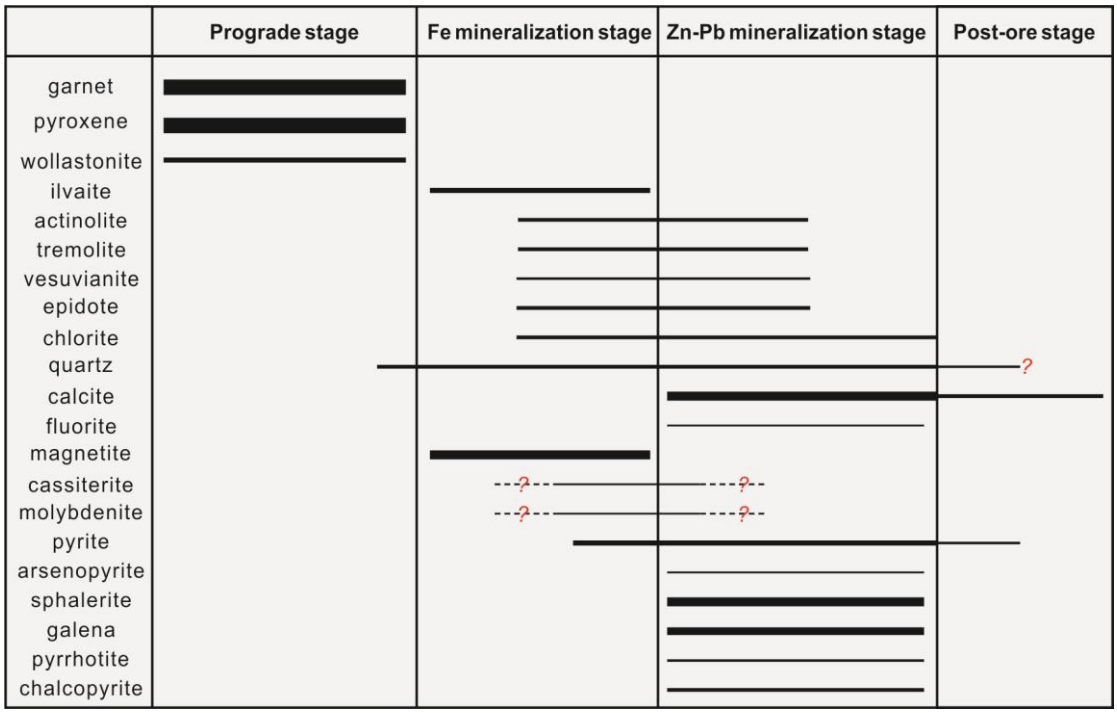

Figure S3 Schematic paragenetic sequence of the Haobugao Zn-Pb deposit.

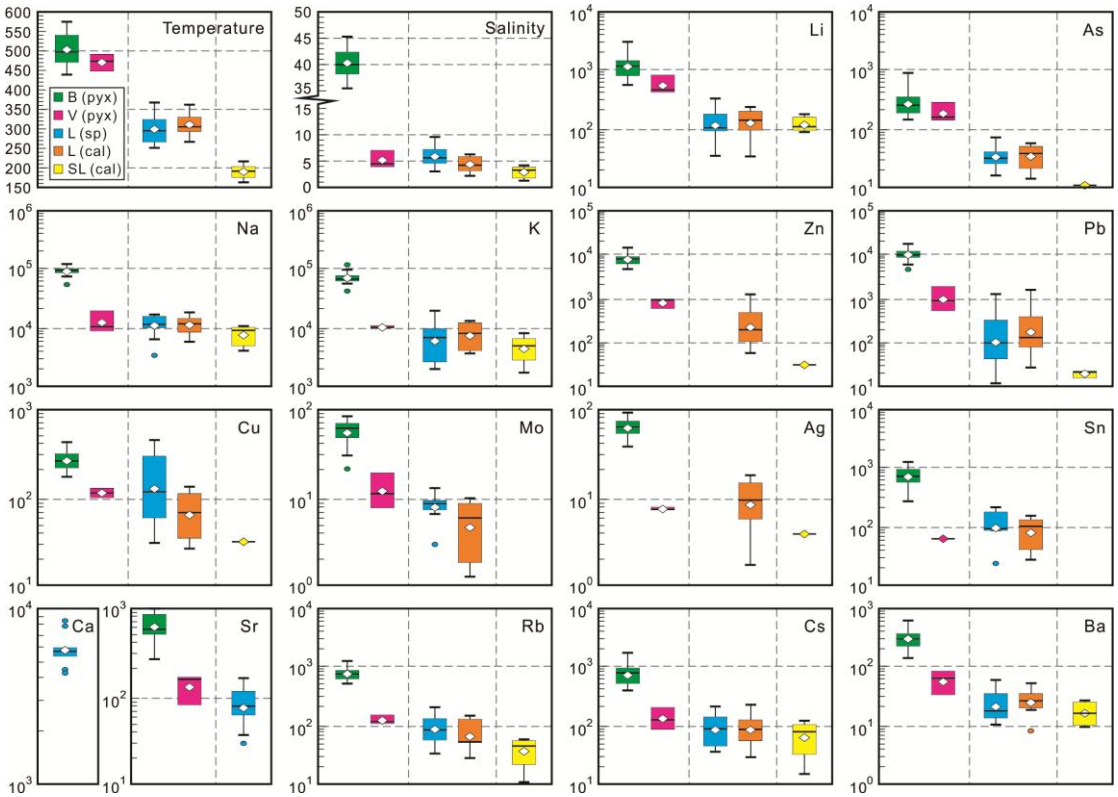

Figure S4 Tukey box plots for temperature (℃), salinity (wt% NaCl equivalent) and element concentrations (ppm) of different types of fluid inclusion assemblages in different paragenetic stages. In these box-whisker plots, the top and bottom of boxes represent respectively the 25th to 75th percentile of the data, i.e., the interquartile range (IQR). The bold horizontal line in a box represents the median. The diamonds represent the means of the data. The horizontal lines at the end of each whisker represent the ends of the 1.5 IQR range beyond the IQR. Circles beyond the whiskers are outliers that exceed the IQR by a factor of 1.5 to 3.

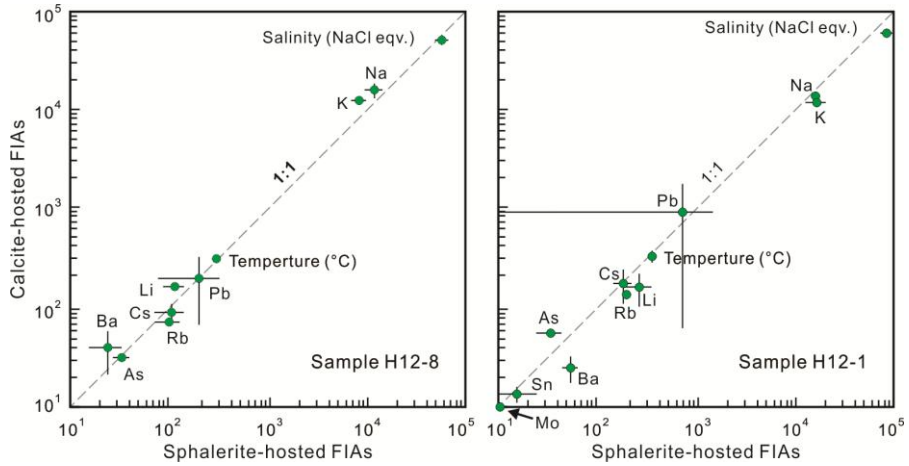

Figure S5 Comparisons of temperatures, salinities and element concentrations (in ppm) between sphalerite-hosted and coexistent calcite-hosted Type L FIAs in samples H12-8 and H12-1, showing that the fluid properties in both minerals are similar, further confirming that the Zn-Pb mineralization stage calcite and sphalerite in Haobugao were precipitated from the same fluids.

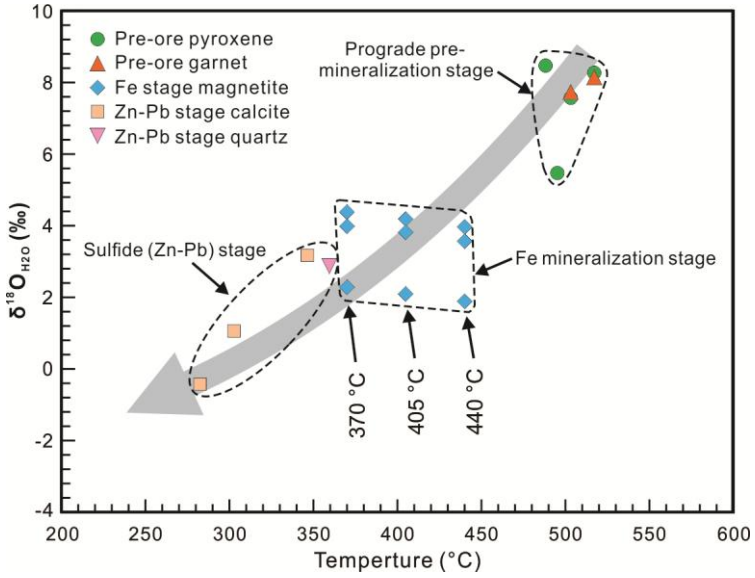

Figure S6 Plot of calculated $\delta^{18}O$ compositions of fluid in equilibrium with minerals from prograde stage through Fe mineralization stage to sulfide stage. The temperature values are based on fluid inclusion microthermometric results in the corresponding minerals in prograde and sulfide stages. For the Fe stage, due to the lack of available fluid inclusion microthermometric data, the temperature is assumed to be lower than the prograde stage but higher than the sulfide stage, i.e., 370–440 ℃; for each analysis, the $\delta^{18}O_{H2O}$ value was calculated at 370, 405 and 440 ℃ to cover the full possible temperature range.

References cited above

Allan, M.M., Yardley, B.W., Forbes, L.J., Shmulovich, K.I., Banks, D.A., and Shepherd, T.J., 2005, Validation of LA-ICP-MS fluid inclusion analysis with synthetic fluid inclusions: American Mineralogist, v. 90, p. 1767–1775, https://doi.org/10.2138/am.2005.1822.

Guillong, M., Meier, D.L., Allan, M.M., Heinrich, C.A., and Yardley, B.W.D., 2008, SILLS: a MATLAB-based program for the reduction of laser ablation ICP-MS data of homogeneous materials and inclusions, in Sylvester, P., ed., Laser Ablation ICP-MS in the Earth Sciences: Current Practices and Outstanding Issues: Mineralogical Association of Canada, Short Course Series, v. 40, p. 328–333 (Vancouver).

Halter, W.E., Pettke, T., Heinrich, C.A., and Rothen-Rutishauser, B., 2002, Major to trace element analysis of melt inclusions by laser-ablation ICP-MS: methods of quantification: Chemical Geology, v. 183, p. 63-86, https://doi.org/10.1016/S0009-2541(01)00372-2.

Hammerli, J., Rusk, B., Spandler, C., Emsbo, P., Oliver, N.H.S., 2013, In situ quantification of Br and Cl in minerals and fluid inclusions by LA-ICP-MS: a powerful tool to identify fluid sources: Chemical Geology, v. 337–338, p. 75–87, https://doi.org/10.1016/j.chemgeo.2012.12.002.

Li, J.F., 2015, Mineralization and periphery metallogenic prediction of the Hongling Pb-Zn polymetallic deposit in Chifeng, Inner Mongolia: PhD thesis, Jilin University, Changchun, China, 202 p (available online; in Chinese with English abstract).

Liu, L., Zhou, T., Zhang, D., et al., 2018, S isotopic geochemistry, zircon and cassiterite U-Pb geochronology of the Haobugao Sn polymetallic deposit, southern Great Xing'an Range, NE China: Ore Geology Reviews, v. 93, 168–180, https://doi.org/10.1016/j.oregeorev.2017.12.008.

Shu, Q., Chang, Z., Hammerli, J., Lai, Y., and Huizenga, J-M., 2017, Composition and evolution of fluids forming the Baiyinnuo'er skarn Zn-Pb deposit, northeastern China: insights from laser ablation ICP-MS study of fluid inclusions: Economic Geology and the Bulletin of the Society of Economic Geologists, v. 112, p. 1441–1460, https://doi.org/10.2113/econgeo.108.4.835.

Steele-MacInnis, M., Lecumberri-Sanchez, P., and Bodnar, R.J., 2012, Short note: HOKIEFLINCS_H_2O-NaCl: a Microsoft Excel spreadsheet for interpreting microthermometric data from fluid inclusions based on the PVTX properties of H_2O-NaCl: Computers & Geosciences, v. 49, p. 334–337, https://doi.org/10.1016/j.cageo.2012.01.022.